NANO LETTERS

2007
Vol. 7, No. 11
3360−3365

Two-Dimensional Imaging by Far-Field Superlens at Visible Wavelengths

Yi Xiong, Zhaowei Liu, Cheng Sun, and Xiang Zhang*

5130 Etcheverry Hall, NSF Nanoscale Science and Engineering Center (NSEC), University of California, at Berkeley, Berkeley, California 94720

Received July 7, 2007; Revised Manuscript Received September 5, 2007

ABSTRACT

We report that two-dimensional (2D) sub-diffraction-limited images can be theoretically reconstructed by a new metamaterial far-field superlens. The metamaterial far-field superlens, composed of a metal–dielectric multilayer and a one-dimensional (1D) subwavelength grating, can work over a broad range of visible wavelengths intrinsically. The imaging principle and the reconstruction process are described in detail. The 2D sub-diffraction-limited imaging ability enables more applications of the far-field superlens in optical nanoimaging and sensing.

The resolution of conventional optical microscope is limited to about half of the wavelength of the illumination light due to the absence of the evanescent waves in the far field that carry the high spatial frequency information. This resolution limit is well-known as the diffraction limit. It is of great interest to realize optical microscopes with sub-diffraction-limited resolution due to the numerous demands in nanoscience and nanotechnology. Near-field scanning optical microscope (NSOM) breaks the diffraction limit[1,2] by scanning a sharp tip in the near field of the object and collecting the evanescent wave information. Stimulated emission depletion (STED) microscope[3] is another technique to overcome the diffraction limit by utilizing stimulated emission to sharpen the fluorescence focal spot. However both techniques require the time-consuming point-by-point scanning process, which prevents them from real-time imaging. Nonlinear structured illumination microscopy[4] has relatively faster imaging speed but requires nonlinear response of the material.

Recently, Pendry proposed that a slab of left-handed material could theoretically form a real-time image without any resolution limit.[5] Metamaterials composed of artificial structures have been commonly used to realize such left-handed material because it does not exist in nature. In spite of the significant advancement toward high frequency,[6−11] the realization of the left-handed material at optical range remains challenging. Alternatively, a thin slab of material with negative permittivity, termed superlens, can be used to form sub-diffraction-limited images for TM polarization without scanning over the object.[5,12,13] The concept was proved experimentally at near-UV and IR wavelength by using silver[14,15] and silicon carbide[16] film, respectively. Unfortunately, it was pointed out that the superlens could only produce sub-diffraction-limited images in the near field.[17] Therefore, an optical microscope capable of projecting sub-diffraction-limited images to the far field is in great demand. The work of optical hyperlens[18−21] has shown remarkable advance toward this goal. Another exciting technique, called optical far-field superlens (FSL), has also shown great potential, and the one-dimensional (1D) sub-diffraction-limited image in the far field has been successfully demonstrated.[22,23] The FSL is made of a silver slab and a 1D subwavelength grating. The silver slab of the FSL enhances the evanescent waves and the subwavelength grating of the FSL converts the enhanced evanescent waves into the propagating waves so that the high spatial frequency information can be collected in the far field, and the sub-diffraction-limited images can be consequently reconstructed. The FSL solves the problem that the superlens only forms the sub-diffracted-limited images in the near field while keeping the advantage of the superlens so that no scanning process is needed. In the present work, we report two-dimensional (2D) imaging by the FSL. The 2D sub-diffraction-limited images are obtained by rotating a metamaterial FSL, which can work over a broad range of visible wavelengths intrinsically. In the following, the imaging principle and the reconstruction process will be described in detail.

In Figure 1a, the red region represents the propagating band of a 2D object, which can be detected in the far field. (Here we only consider half of the propagating band. The other half can be treated similarly.) The inset is the schematic of a metamaterial FSL, which is comprised of a metal−dielectric multilayer and a 1D subwavelength metal−dielectric grating (we will discuss why a multilayer structure is used, how it works, and how the multilayer structure is designed later). When the periodic direction of

* Corresponding author. E-mail: xiang@berkeley.edu.

10.1021/nl0716449 CCC: $37.00
Published on Web 10/05/2007

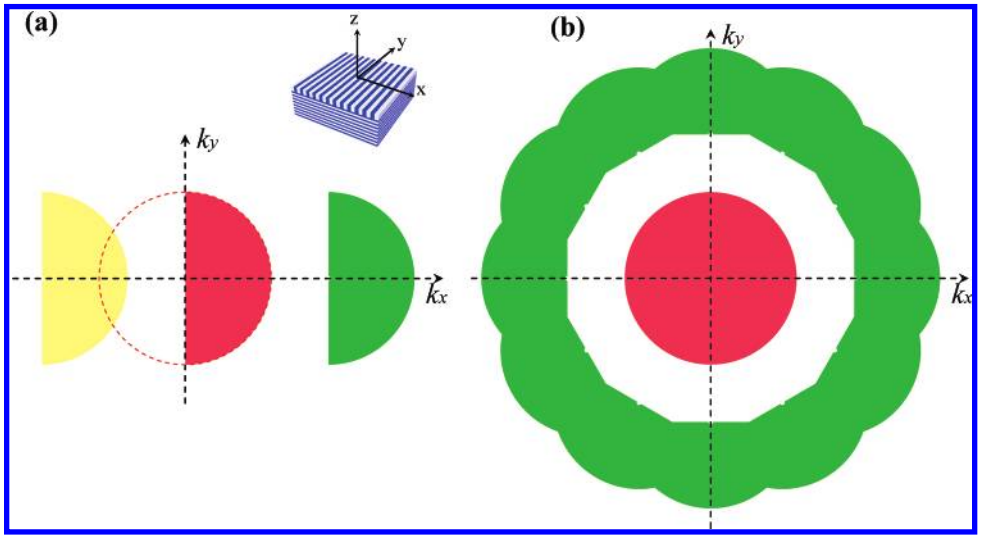

Figure 1. Principle of 2D imaging by FSL. (a) Three contributions to half of the propagating band after the FSL: the 0 order, −1 order, and +1 order diffraction waves of the incident waves with wavevectors within the red, green, and yellow region respectively. The region within the red dashed circle is the propagating band. (b) The information in the green ring region can be retrieved from far-field measurements with six orientations of the FSL. The information of the red region (propagating band) can be obtained from measurement using a reflection mode of a conventional optical microscope.

the subwavelength grating is along the *x* direction, as shown in Figure 1a, the grating only provides wavevectors in the k_x direction. Therefore the propagating waves after the FSL have three contributions: the 0 order, −1 order, and +1 order diffraction waves of the incident waves with wavevectors within the red, green, and yellow region in Figure 1a, respectively. (The incident waves are the scattering waves from the 2D object at the plane immediately before the FSL. Higher diffraction orders are neglected due to small diffraction efficiency.) The FSL is designed in a way that the propagating part of the diffracted waves after the FSL mainly comes from the −1 order diffraction of the incident waves with wavevectors within the green region in Figure 1a. Then by measuring the spectrum of the propagating waves after the FSL, the information of the incident waves with wavevectors within the green region in Figure 1a can be retrieved. To reconstruct a 2D high-resolution image, the information in all directions is required. Naturally, a straightforward solution is to rotate the FSL to obtain the information in all directions. For example, one can rotate the FSL by 30° (along the *z*-axis in Figure 1a), and then the information of another green region can be retrieved from the spectrum of the propagating waves measured in the far field after the FSL. By accumulating measurements from six orientations of the FSL, one can obtain the information in the green ring as shown in Figure 1b (in each measurement, information in two symmetric green region is retrieved when both half propagation bands are considered). The propagating information of the incident waves within the red region in Figure 1b can be obtained by a reflection mode of a conventional optical microscope. As a result, a 2D sub-diffraction-limited image can be reconstructed from the retrieved spectrum.

In our previous work,[22,23] the FSL consisted of a silver slab and a 1D silver−dielectric grating has successfully demonstrated the 1D imaging by designing a specific optical transfer function based on the surface plasmon resonance excitation. Instead of using the previous FSL in general 2D imaging, we present a new FSL design with significantly improved performance in the following two crucial aspects. The first aspect is the signal dominancy for the −1 diffraction order. In our previous FSL design, the transfer function for −1 order is about 1 order of magnitude larger than that of the rest, which, in return, requires that the amplitudes of the propagating components in the object spectrum are comparable or smaller than those of the evanescent components. To free this constraint of the objects, the transfer function ratio between the dominant order and the rest has been improved by a couple of orders in the new FSL design. The second aspect is the designability of the enhanced evanescent band at visible wavelengths. In the FSL in refs 22 and 23, the evanescent waves over a broad wavevector band are enhanced simultaneously due to the surface plasmon resonance excitation at the condition $|\epsilon_m| \approx \epsilon_d$. ϵ_m and ϵ_d are permittivities of metal and dielectric respectively. Therefore, once the materials are fixed, the enhanced evanescent band and the working wavelength are fixed as well. In contrast, the new FSL has the flexibility of designing the location and bandwidth of the enhanced evanescent wave band at desired visible wavelength.

This new designed FSL is composed of a metal−dielectric multilayer, termed a flat metamaterial superlens, and a 1D subwavelength grating. Similar to the original FSL, the flat metamaterial superlens enhances the evanescent waves and attenuates the propagating waves, while the subwavelength grating converts the enhanced evanescent waves into propagating waves so that the information carried by evanescent waves can be detected and retrieved in the far field.

Macroscopically, the fact that the flat metamaterial superlens enhances the evanescent waves and attenuates the propagating waves can be explained by the dispersion relation of the metal−dielectric multilayer using effective medium theory when the film thickness is much smaller than

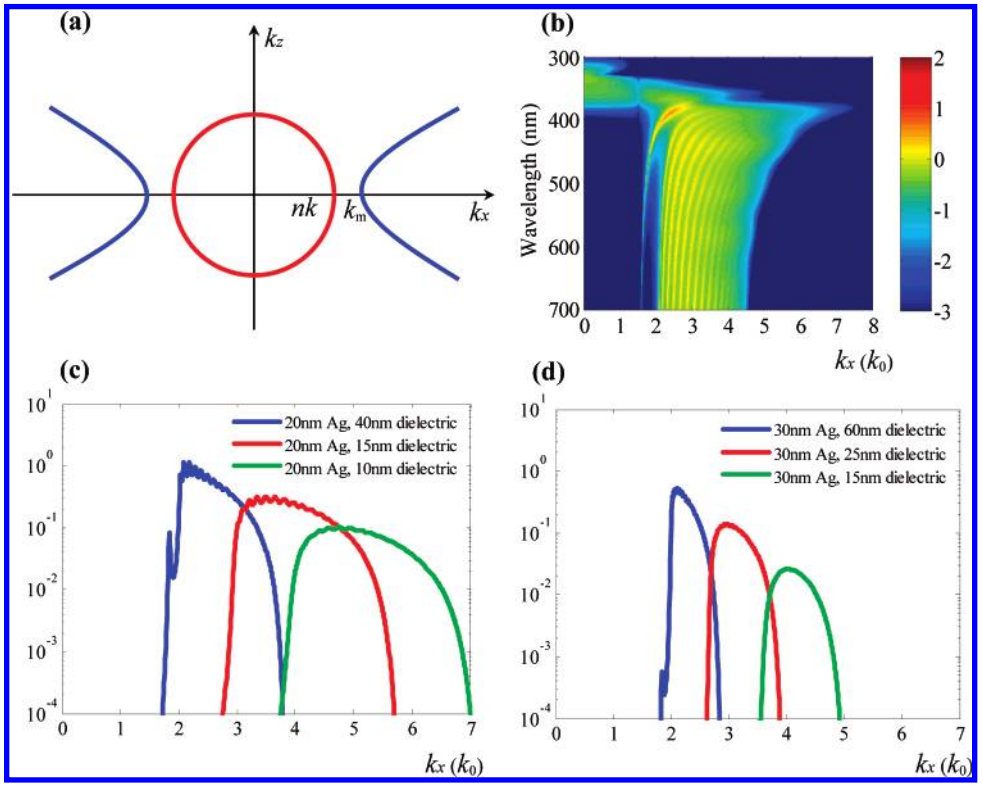

Figure 2. (a) Dispersion relation of a metal−dielectric multilayer with $\epsilon_{\text{eff},z} > 0$, $\epsilon_{\text{eff},x} < 0$. (b) Calculated transmission coefficients (in logarithm scale) of 20 pairs of 15 nm Ag and 20 nm dielectric multilayer. Permittivity of Ag is obtained from ref 24, while permittivity of dielectric is 2.28. (c) Calculated transmission coefficients (in logarithm scale) of 30 pairs of Ag (thickness of each Ag layer is 20 nm) and dielectric (wavelength is 450 nm). (d) Calculated transmission coefficients (in logarithm scale) of 30 pairs of Ag (thickness of each Ag layer is 30 nm) and dielectric (wavelength is 450 nm).

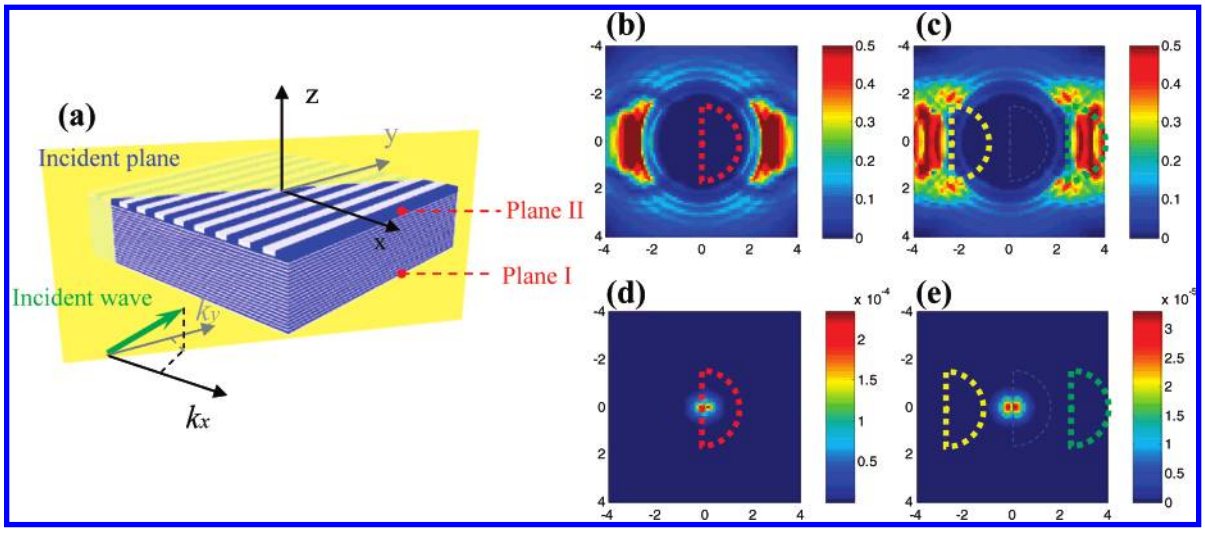

Figure 3. Two-dimensional transfer functions of a metamaterial FSL (the metamaterial FSL is made of 20 pairs of 15 nm Ag/20 nm dielectric ($\epsilon = 2.28$) and a 1D Ag−dielectric subwavelength grating. The thickness, period, and Ag filling ratio of the subwavelength grating are 55 nm, 160 nm, and 0.3, respectively. The working wavelength is 405 nm). (a) Schematic of the incident wave with respect to the metamaterial FSL. (b,c) Zero and first-order transfer function for p-polarization. (d,e) Zero and first-order transfer function for s-polarization. The unit in both horizontal and vertical axis are k_0. Notice the color scale difference between (b,c) and (d,e).

the working wavelength. For TM polarization, the dispersion relation of a metal−dielectric multilayer is $k_x^2/\epsilon_{\text{eff},z} + k_z^2/\epsilon_{\text{eff},x} = k_0^2$, where $\epsilon_{\text{eff},x} = p\epsilon_{\text{metal}} + (1 - p)\epsilon_{\text{dielectric}}$, $\epsilon_{\text{eff},z} = (\epsilon_{\text{metal}}\epsilon_{\text{dielectric}})/((1 - p)\epsilon_{\text{metal}} + p\epsilon_{\text{dielectric}})$, p is the filling ratio of metal layer. The isofrequency contour is shown in Figure 2a when $\epsilon_{\text{eff},z} > 0$, $\epsilon_{\text{eff},x} < 0$. The isofrequency contour curve indicates that the multilayer structure only supports propagation for incident waves with wavevectors larger than k_m.

Microscopically, the special transmission property of the metal−dielectric multilayer can be explained by a surface plasmon mode interaction picture. The mechanism of simultaneous enhancement of evanescent waves within a broad

range of wavevectors by the multilayer is different from that of the silver slab. It is well-known that surface plasmon modes split on metal thin film due to the interaction of modes on two metal surfaces.[25] As the number of the metal thin films increases, the number of the split surface plasmon modes increases accordingly. With proper design, the split surface plasmon modes can be highly compact. Then the transmission of the evanescent waves through the multilayer is large over a continuously broad range of wavevectors (Figure 2b shows the transmission coefficient through a metal−dielectric multilayer). On the other hand, the transmission of the propagating waves through the multilayer is lower due to the increased total thickness of the metal. Therefore, the transmission ratio of the evanescent waves and the propagating waves through the multilayer is significantly increased compared with that of the silver slab. As a result, the −1 order transfer function of the metamaterial FSL can be several orders larger than the 0 and +1 order transfer functions. In addition, because the enhancement of the evanescent waves by metal−dielectric multilayer is due to the splitting of surface plasmon mode instead of the surface plasmon resonance excitation at the condition $|\epsilon_m| \approx \epsilon_d$,[26] the metamaterial FSL can work over a broad range of wavelengths, which is absolutely favorable in various imaging applications.

Figure 2b, calculated transmission coefficients (in logarithm scale) of a Ag−dielectric multilayer, shows that the transmission of evanescent waves due to the surface plasmon mode splitting in the multilayer is at least 3 orders larger than the transmission of propagating waves. It also shows that evanescent waves are simultaneously enhanced over a broad wavevector range and a wide range of wavelengths. It is worth mentioning that the location and the bandwidth of the enhanced transmission wavevector band can be tuned by changing the thickness of the Ag and dielectric layer (see Figure 2c,d for examples), which adds flexibility of enhancing the desired evanescent band.

For 2D imaging, we extend the transfer functions concept in refs 22 and 23 to 2D transfer functions. For a given set of k_x and k_y, the −1 order transfer function is defined as the wave amplitude ratio between the −1 order diffracted waves at plane II and the incident waves at plane I in Figure 3a (0 order and +1 order transfer functions are defined similarly). k_x and k_y are tangential wavevectors of incident waves (incident waves are the scattering waves from the 2D object at the plane immediately before the metamaterial FSL [plane I in Figure 3a]). Parts b−e of Figure 3 show the 2D transfer functions of a metamaterial FSL, which were calculated by 2D rigorous coupled wave analysis (RCWA).[27,28] Parts b and c and parts d and e of Figure 3 show transfer functions for p-polarization and s-polarization, respectively. Each set of k_x and k_y in Figure 3 is associated with an incident plane as shown in Figure 3a. The p-polarization is the case that incident H-field is perpendicular to the incident plane. Therefore, the direction of incident H-field is different for different set of k_x and k_y (Similarly s-polarization can be defined by replacing H with E). In real experiment, the illumination light can be unpolarized so that the metamaterial FSL automatically selects the p-polarized direction for each set of k_x and k_y and allows its transmission. In the first-order transfer function figures (Figure 3c,e), when $k_x \geq 0$, the transfer function is −1 order transfer function; while when $k_x < 0$, it is the +1 order transfer function. It can be seen that −1 order transfer function for incident waves in the green dashed region in Figure 3c is 3 orders larger than the +1 order transfer function for incident waves in the yellow dashed region in Figure 3c and the 0 order transfer function for incident waves in the red dashed region in Figure 3b.

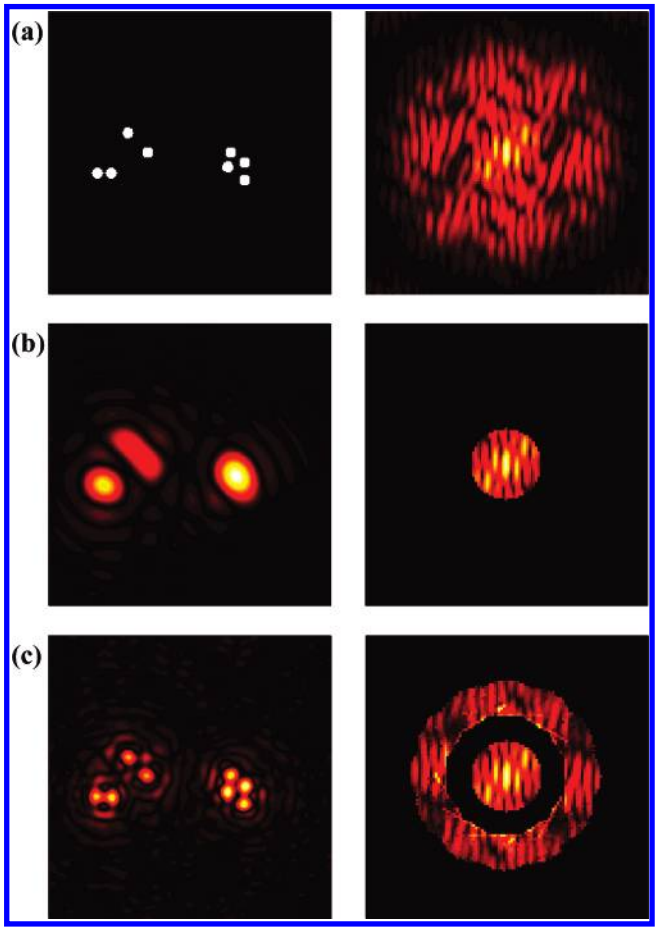

Figure 4. Numerical demonstration of 2D imaging with sub-diffraction-limited resolution by the metamaterial FSL. The working wavelength is 405 nm. The metamaterial FSL is the same as the one in Figure 3. (a) Sub-diffraction-limited object (the view size is 2 μm by 2 μm) and its spectrum. The object is composed of eight circles with radius of 40 nm. H-field is 1 within each circle and is 0 anywhere else. The center-to-center distances between the eight circles range from 100 to 1059 nm. (b) Simulated real space image obtained by a conventional far-field optical system with NA = 1.5 (diffraction limit: 268 nm) and its spectrum (only the part $k < 1.5\ k_0$ is shown). (c) Image reconstructed by rotating a metamaterial FSL and its restored spectrum.

One 2D sub-diffraction-limited object was employed to show the 2D imaging performance of the new proposed metamaterial FSL. Figure 4a shows the H-field of the 2D object and its spatial spectrum. For a conventional optical microscope with NA = 1.5, the diffraction-limited image and its corresponding spatial spectrum are shown in Figure 4b. The diffraction-limited image is obtained by inverse

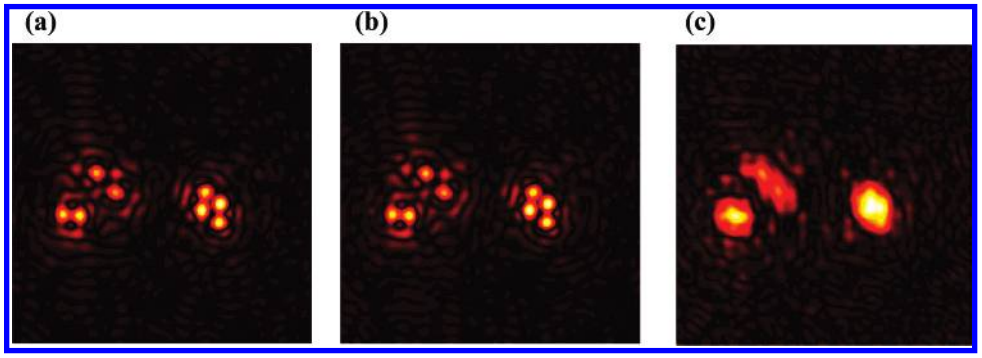

Figure 5. Image reconstructed at wavelength (a) 500 nm, (b) 600 nm, and (c) 365 nm. The metamaterial FSLs and the objects are the same as those in Figure 4 except that the objects and the periods of the gratings in the metamaterial FSLs are scaled by the ratio of wavelengths (for example, at wavelength 500 nm, the object is scaled by the factor 500/405, and the period of the grating is changed from 160 to 200 nm). At wavelength 365 nm, the object can not be correctly reconstructed because the transmissions of the evanescent waves through the multilayer are comparable with those of the propagating waves.

Fourier transform of the propagating band of the 2D object. Obviously, the sub-diffraction-limited features are not distinguishable. The reconstructed image utilizing the metamaterial FSL in Figure 3 is shown in Figure 4c. The reconstructed image is obtained by following the foregoing procedure of six measurements and a reflection mode measurement except that the far-field data that could be measured experimentally is calculated by forward 2D RCWA simulation, that is, the computation of the propagating component of the scattering spectrum after the metamaterial FSL. The eight circular objects are clearly resolved in the reconstructed image utilizing metamaterial FSL. The working wavelength is 405 nm, and the smallest center-to-center distance is 100 nm. The artificial dots in Figure 4c are due to the missing information between the propagating band and reconstructed evanescent band.

As mentioned before, the advantage of the metamaterial FSL is that the working wavelength can be changed to other visible wavelengths. Figure 5 shows the images reconstructed at different wavelengths. The metamaterial FSLs and the objects in Figure 5 are the same as those in Figure 4 except that the objects and the periods of the gratings in the metamaterial FSLs are scaled by the ratio of wavelengths (for example, at wavelength 500 nm, the object is scaled by the factor 500/405 and the period of the grating is changed from 160 to 200 nm). At 500 and 600 nm wavelengths, the sub-diffraction-limited objects are clearly reconstructed as shown in Figure 5a,b. A wavelength of 365 nm is not a suitable working wavelength of the metamaterial FSL because the transmissions of the evanescent waves through the multilayer are comparable with those of the propagating waves (refer to Figure 2b). Consequently, the objects cannot be correctly reconstructed, as shown in Figure 5c.

To experimentally realize 2D sub-diffraction-limited imaging by rotating a metamaterial FSL, one should have the ability to fabricate the metamaterial FSL, to control the rotation of the metamaterial FSL and to measure both the phase and amplitude of the diffraction waves after the metamaterial FSL, which are all feasible considering current fabrication and calibration techniques. We should also mention that the view size of this method is not limited by the view sizes used in the current simulations.

In conclusion, we reported that theoretically 2D sub-diffraction-limited images could be reconstructed by rotating a metamaterial FSL, which intrinsically could work over a broad range of visible wavelengths. The 2D sub-diffraction-limited imaging ability enables more applications of FSL in nanoscale optical imaging and sensing.

Acknowledgment. This work was supported by the Army Research Office Multidisciplinary University Research Initiative (MURI) program (grant no. 50432-PH-MUR) and the NSF NSEC under award no. DMI0327077.

References

(1) Synge, E. H. *Philos. Mag.* **1928**, *6*, 356−362.
(2) Betzig, E.; Trautman, J. K.; Harris, T. D.; Weiner, J. S.; Kostelak, R. L. *Science* **1991**, *251*, 1468−1470.
(3) Hell, S. W.; Wichmann, J. *Opt. Lett.* **1994**, *19*, 780−782.
(4) Gustafsson, M. G. L. P. *Proc. Natl. Acad. Sci. U.S.A.* **2005**, *102*, 13081−13086.
(5) Pendry, J. B. *Phys. Rev. Lett.* **2000**, *85*, 3966−3969.
(6) Podolskiy, V. A.; Sarychev, A. K.; Shalaev, V. M. *Opt. Express* **2003**, *11*, 735−745.
(7) Yen, T. J.; Padilla, W. J.; Fang, N.; Vier, D. C.; Smith, D. R.; Pendry, J. B.; Basov, D. N.; Zhang, X. *Science* **2004**, *303*, 1494−1496.
(8) Linden, S.; Enkrich, C.; Wegener, M.; Zhou, J.; Koschny, T.; Soukoulis, C. M. *Science* **2004**, *306*, 1351−1353.
(9) Zhang, S.; Fan, W. J.; Minhas, B. K.; Frauenglass, A.; Malloy, K. J.; Brueck, S. R. *J. Phys. Rev. Lett.* **2005**, *94*, 037402.
(10) Kwon, D. H.; Werner, D. H.; Kildishev, A. V.; Shalaev, V. M. *Opt. Express* **2007**, *15*, 1647−1652.
(11) Lezec, H. J.; Dionne, J. A.; Atwater, H. A. *Science* **2007**, *316*, 430−432.
(12) Fang, N.; Zhang, X. *Appl. Phys. Lett.* **2003**, *82*, 161−163.
(13) Blaikie, R. J.; McNab, S. J. *Microelectron. Eng.* **2002**, *61*−*62*, 97−103.
(14) Fang, N.; Lee, H.; Sun, C.; Zhang, X. *Science* **2005**, *308*, 534−537.
(15) Melville, D. O. S.; Blaikie, R. J. *Opt. Express* **2005**, *13*, 2127−2134.
(16) Taubner, T.; Korobkin, D.; Urzhumov, Y.; Shvets, G.; Hillenbrand, R. *Science* **2006**, *313*, 1595−1595.
(17) Podolskiy, V. A.; Narimanov, E. E. *Opt. Lett.* **2005**, *30*, 75−77.
(18) Jacob, Z.; Alekseyev, L. V.; Narimanov, E. *Opt. Express* **2006**, *14*, 8247−8256.
(19) Salandrino, A.; Engheta, N. *Phy. Rev. B* **2006**, *74*, 075103.
(20) Liu, Z. W.; Lee, H.; Xiong, Y.; Sun, C.; Zhang, X. *Science* **2007**, *315*, 1686−1686.
(21) Smolyaninov, I. I.; Hung, Y. J.; Christopher, C. D. *Science* **2007**, *315*, 1699−1701.

(22) Durant, S.; Liu, Z. W.; Steele, J. M.; Zhang, X. *J. Opt. Soc. Am. B* **2006**, *23*, 2383−2392.
(23) Liu, Z. W.; Durant, S.; Lee, H.; Pikus, Y.; Fang, N.; Xiong, Y.; Sun, C.; Zhang, X. *Nano Lett.* **2007**, *7*, 403−408.
(24) Johnson, P. B.; Christy, R. W. *Phys. Rev. B* **1972**, *6*, 4365−4379.
(25) Economou, E. N. *Phys. Rev.* **1969**, *182*, 539−554.
(26) Xiong, Y.; Liu, Z. W.; Durant, S.; Lee, H.; Sun, C.; Zhang, X. *Opt. Express* **2007**, *15*, 7095−7102.
(27) Li, L. F. *J. Opt. Soc. Am. A* **1996**, *13*, 1024−1035.
(28) Li, L. F. *J. Opt. Soc. Am. A* **1997**, *14*, 2758−2767.

NL0716449